1-1979

T-Matrix Calculations for Spheroidal and Crack Like Flaws

Vasundara V. Varadan
Ohio State University

Vijay K. Varadan
Ohio State University

T-Matrix Calculations for Spheroidal and Crack Like Flaws

Abstract
Numerical calculations are presented for the scattering of elastic (P- and S-) waves from prolate and oblate spheroids and two-dimensional, rough, crack-like flaws for various angles of incidence, observation and frequencies using the T-matrix approach.

Keywords
Nondestructive Evaluation

Disciplines
Materials Science and Engineering | Mechanical Engineering

T-MATRIX CALCULATIONS FOR SPHEROIDAL AND CRACK LIKE FLAWS

Vasundara V. Varadan and Vijay K. Varadan
Department of Engineering Mechanics
The Ohio State University
Columbus, Ohio 43210

ABSTRACT

Numerical calculations are presented for the scattering of elastic (P- and S-) waves from prolate and oblate spheroids and two-dimensional, rough, crack-like flaws for various angles of incidence, observation and frequencies using the T-matrix approach.

INTRODUCTION

Previously the T-matrix[1] method has been successfully used for two dimensional elastic scatterers[2,3] for arbitrary scattering geometry and for spheroidal elastic scatterers[4] when a P-wave is incident along the symmetry axis of the spheroid. We have now obtained numerical results for the scattering of P- and S- waves incident at arbitrary angles on prolate and oblate spheroidal cavities and inclusions for a wide range of frequencies.

Some preliminary numerical results have also been obtained for infinitely long cylinders of elliptic cross section when the aspect ratio is very small ~0.07. This will correspond to a two dimensional elliptic crack. For incident SH-waves we have shown that systematic expansions of the T-matrix in powers of ka, a non-dimensional wave number, agree with the exact far field results using matched asymptotic expansions or Mathieu functions for both cavities and inclusions, if the limit of zero aspect ratio is taken in the analytic expressions of the T-matrix. We have also checked the numerical results for aspect ratio ~0.07 against the exact crack results with excellent agreement. We are now incorporating the limiting procedure into the numerical scheme which should make the calculations much more efficient. We will also extend this approach to penny shaped cracks in the near future.

All of these calculations have been made for the purpose of flaw detection in real materials. But real flaws are rarely smooth although most theoretical calculations are based on smooth boundaries. In order to make the scatterer more realistic we have presented some results for the scattering of SH-waves from an elliptic cylinder whose boundary is perturbed by a periodic function. There is considerable difference in the scattering signatures of a rough and smooth surface.

DESCRIPTION OF FIGURES

For spheroidal cavities and inclusions, the host material is taken to be Ti6%Al-4%V and the inclusions are of Tungsten Carbide (WC). The two dimensional results are for Aluminum. A table of material properties follows.

Table I: Material Properties

Material	P-wave velocity	S-wave velocity	Shear modulus
Ti6%Al-4%V	6340 m/s	3030 m/s	4.06×10^{10} N/m^2
WC	6660 m/s	3980 m/s	2.19×10^{11} N/m^2
Aluminum	6420 m/s	3040 m/s	2.5×10^{10} N/m^2

The figures are self descriptive and the scattering geometry for each one of them is clearly indicated. For spheroids, the z-axis is taken as the axis of revolution. For elliptic cylinders, the z-axis coincides with the cylinder axis. 'α' is the angle of incidence measured with respect to the positive z-axis for 3-D geometries and the azimuthal angle is set equal to zero with no loss of generality. The direction of observation is specified by the angles θ, ϕ. For 2-D geometries, the polar angle of incidence, $-\alpha$, and observation, θ, are measured with respect to the positive x-axis which coincides with the major axis of the ellipse.

CONCLUSIONS

These results are yet to be compared with experiments. The data presented here is also being used as a data base for the inversion procedure developed by J. Rose and the adaptive training procedure developed by A. Mucciardi and M. Whalen. The outcome of their calculations should be interesting to see.

ACKNOWLEDGEMENTS:

This research was sponsored by the Center for Advanced NDE, operated by the Science Center, Rockwell International, for the Defence Advanced Research Projects and the Air Force Materials Laboratory under Contract F33615-74-C-5180.

REFERENCES

1. 'Scattering Matrix for Elastic Waves. I. Theory', J. Acoust. Soc. Am. 60, 556 (1976).

2. 'Scattering Matrix for Elastic Waves. II. Application to Elliptic Cylinders', J. Acoust. Soc. Am. 63, 1014 (1978).

3. 'Spectral Analysis of Scattered Elastic Waves', ARPA/AFML Review on Progress in Quantitative NDE, Ithaca, New York (1977).

4. 'Matrix Theory for Elastic Wave Scattering from Spheroids', Sixth Canadian Congress of Applied Mechanics, Vancouver, B.C. (1977).

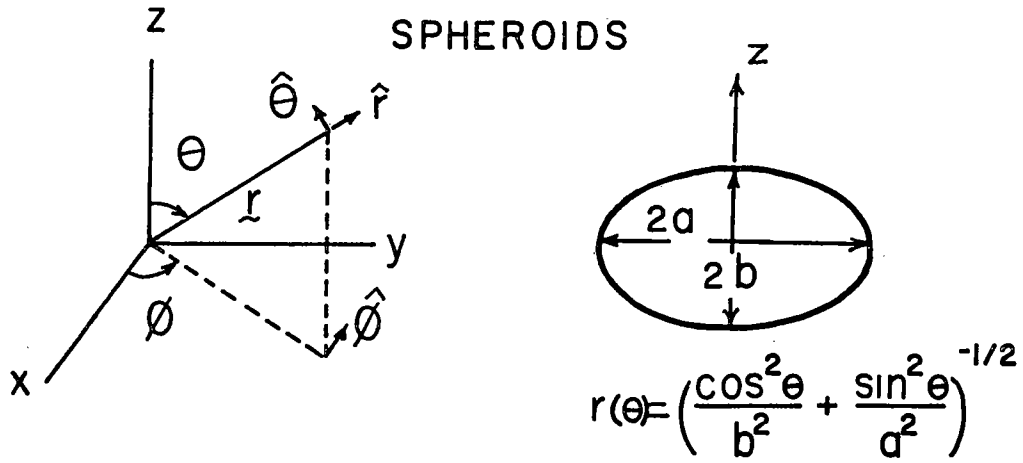

s_1-wave shear wave polarized in $\hat{\theta}$ direction

s_2-wave shear wave polarized in $\hat{\phi}$ direction

s/a - roughness parameter

Fig.1 Notation and geometry

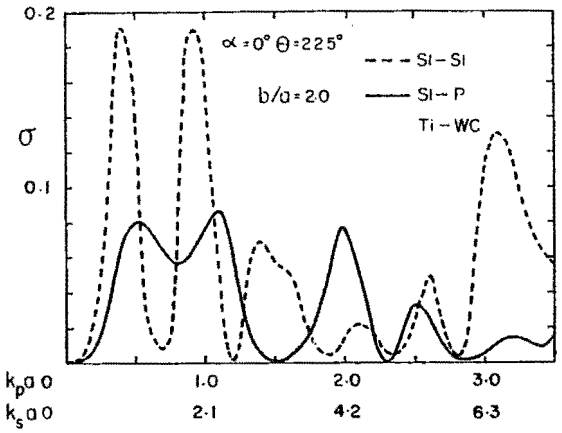

Fig.2 Spectrum of bistatic cross section for Sl - waves incident along symmetry axis of prolate spheroidal inclusion in Ti.

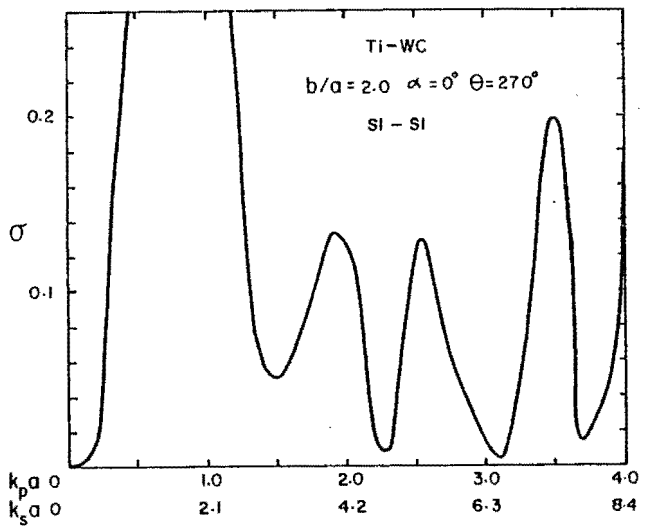

Fig.3 Spectrum of bistatic cross section for Sl - waves incident along symmetry axis of prolate spheroidal inclusion in Ti.

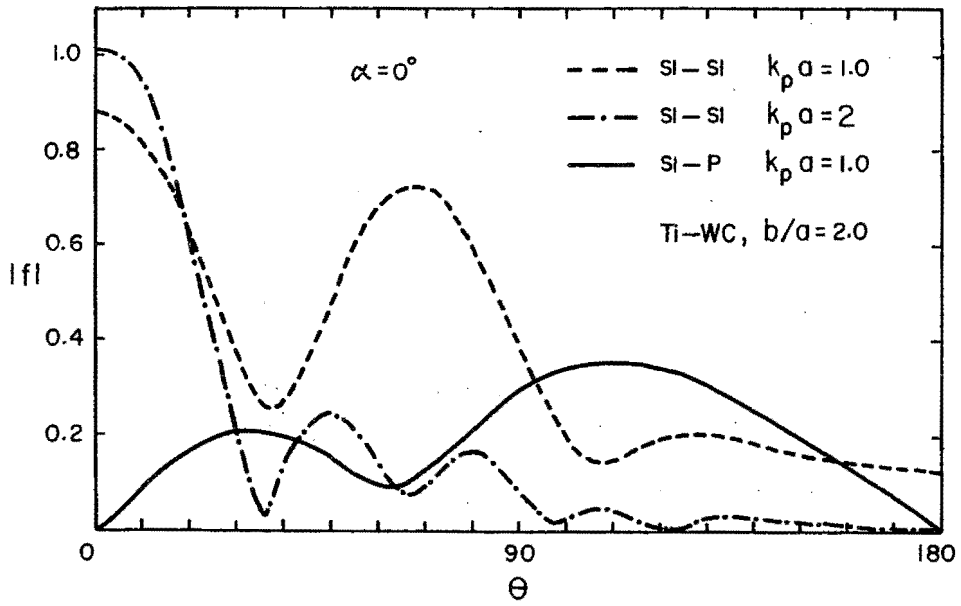

Fig.4 Angular variation of scattered field amplitude for Sl - waves incident at different frequencies along symmetry axis of prolate spheroidal inclusion in Ti.

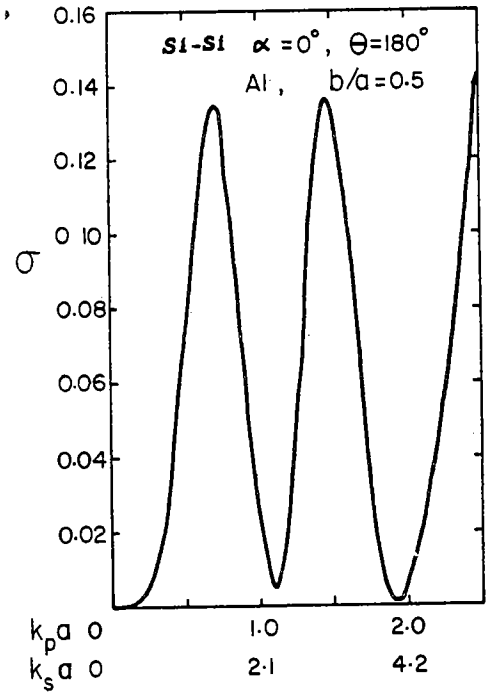

Fig.5 Spectrum of back scattering cross section for P - waves incident along symmetry axis of oblate spheroidal cavity in Al.

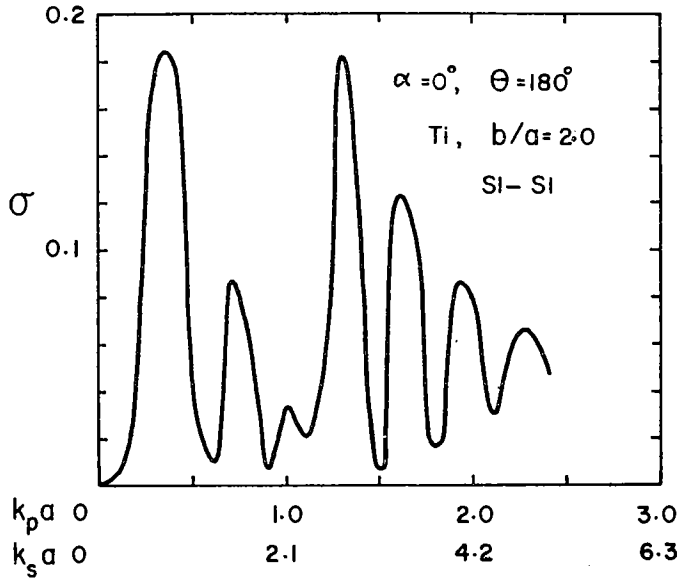

Fig.6 Spectrum of back scattering cross section for Si - waves incident along symmetry axis of prolate spheroidal cavity in Ti.

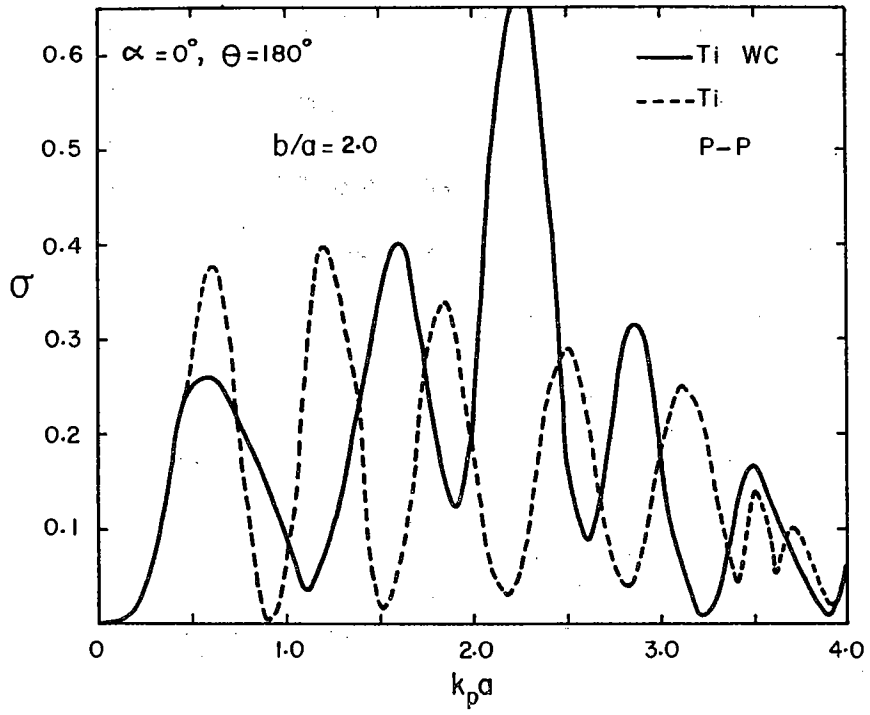

Fig.7 Spectrum of back scattering cross section for P - waves incident along symmetry axis of prolate spheroidal cavity and inclusion in Ti.

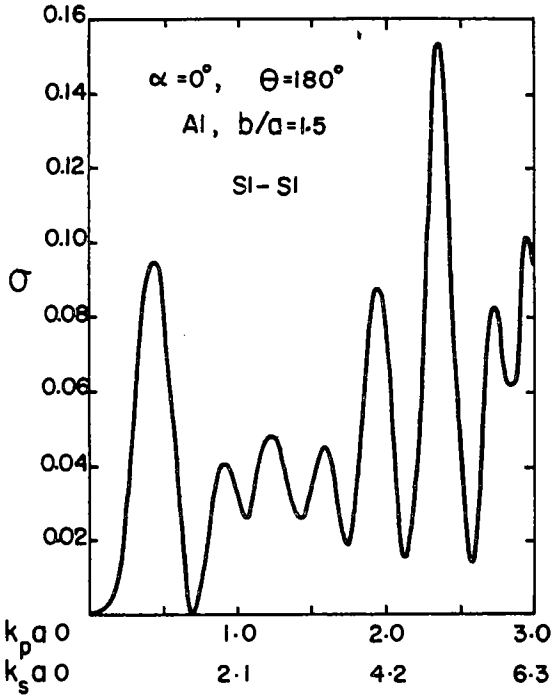

Fig.8 Spectrum of back scattering cross section for Sl - waves incident along symmetry axis of prolate spheroidal cavity in Al.

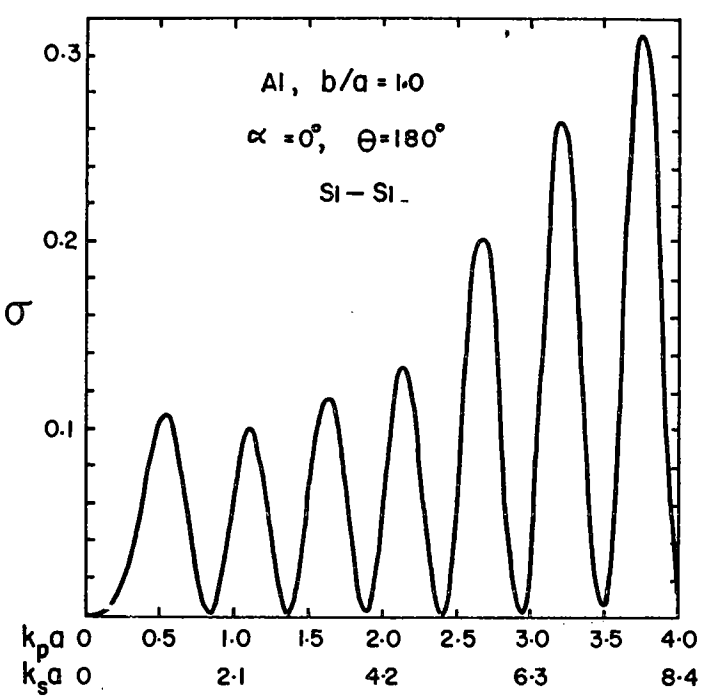

Fig.9 Spectrum of back scattering cross section for Sl - waves incident along symmetry axis of spherical cavity in Al.

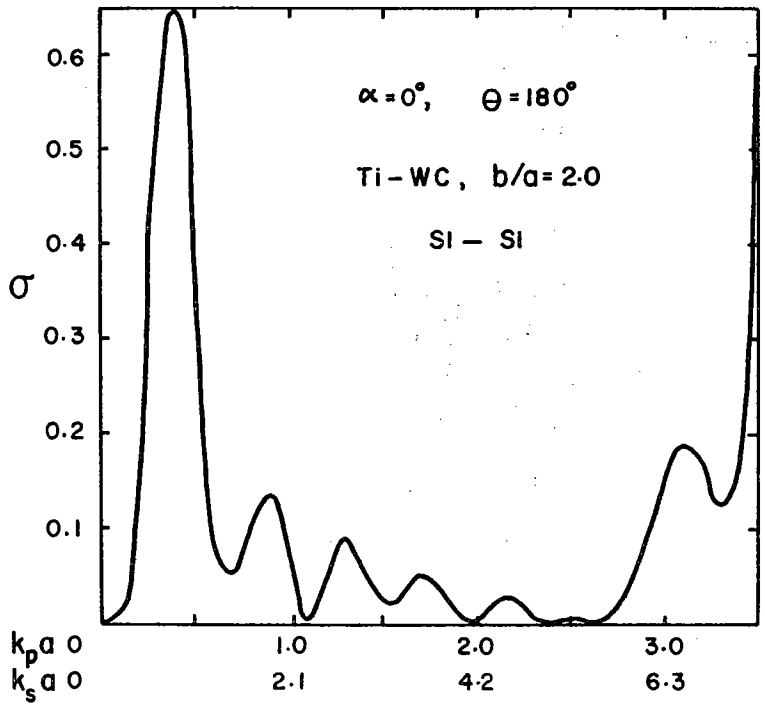

Fig.10 Spectrum of back scattering cross section for Sl - waves incident along symmetry axis of prolate spheroidal inclusion in Ti.

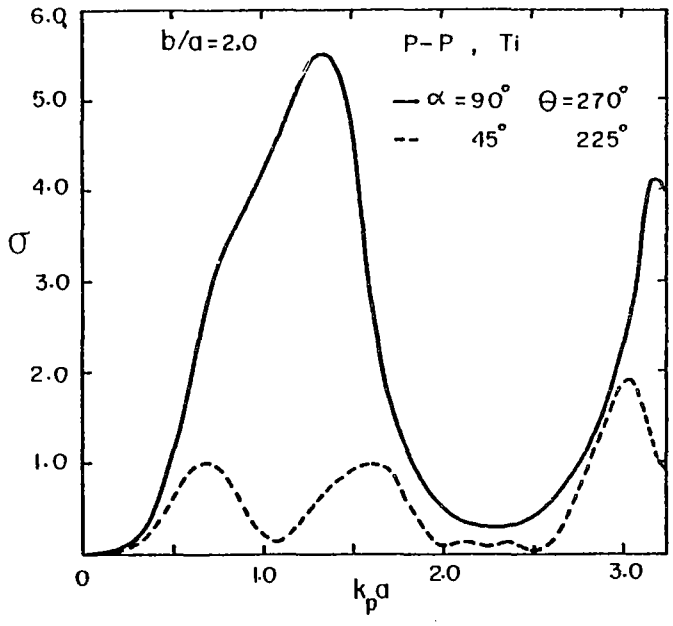

Fig.11 Spectrum of back scattering cross section for P - waves incident at 45 and 90 degrees with respect to symmetry axis of prolate spheroidal cavity in Ti.

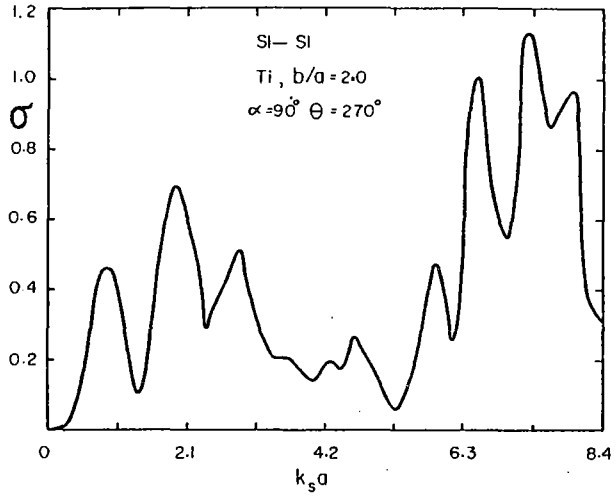

Fig.12 Spectrum of back scattering cross section for SI - waves incident at 90 degrees with respect to symmetry axis of prolate spheroidal cavity in Ti.

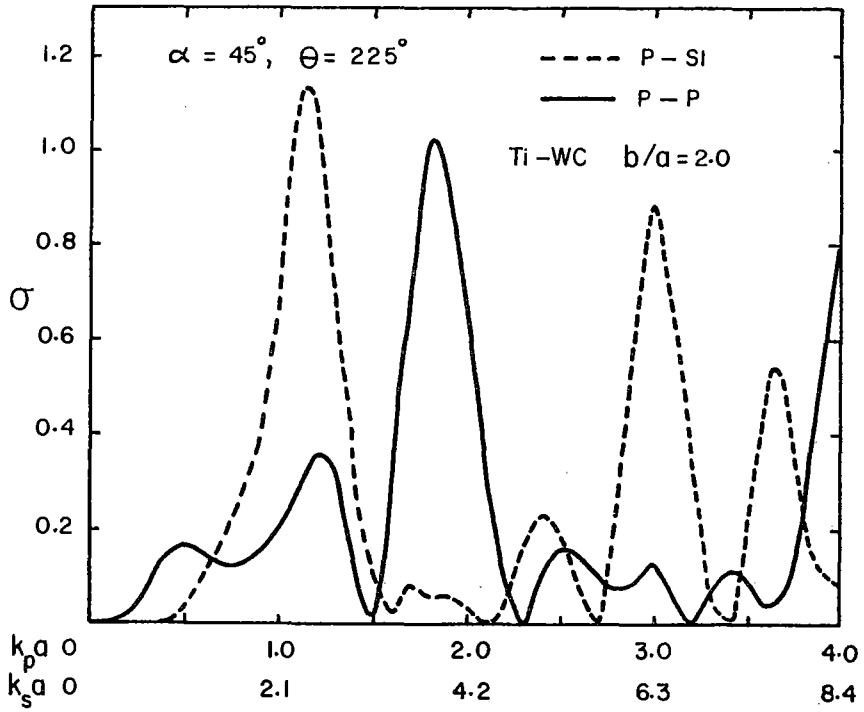

Fig.13 Spectrum of back scattering cross section for P - waves incident at 45 degrees with respect to the symmetry axis of prolate spheroidal inclusion in Ti.

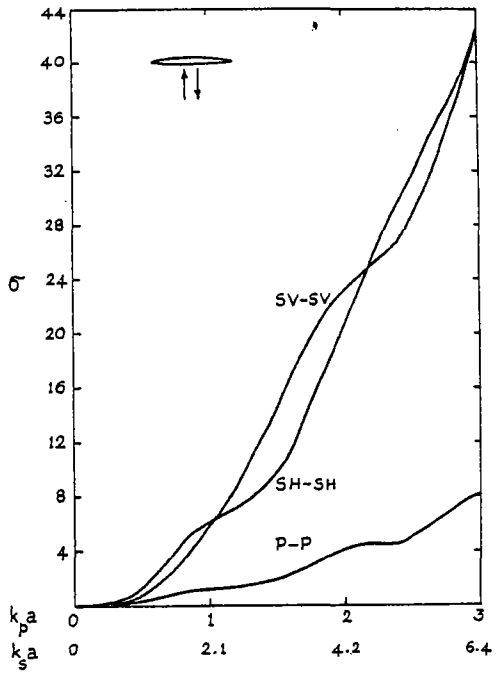

Fig.14 Spectrum of back scattering cross section for P -, SV -, and SH - waves incident normal to an elliptic crack in Al.

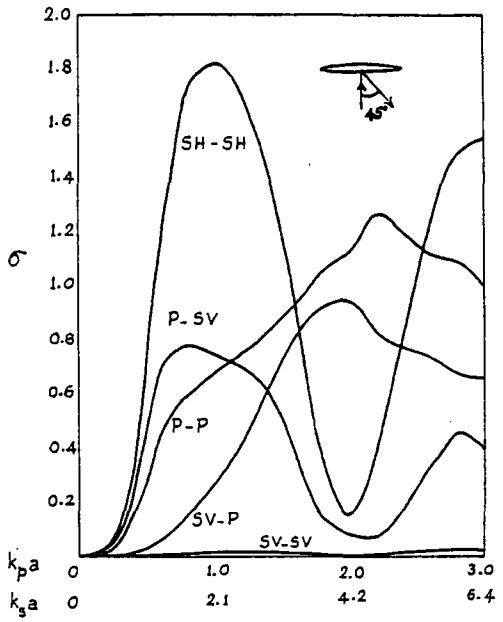

Fig.15 Spectrum of bistatic cross section for P -, SV -, and SH - waves incident normal to an elliptic crack in Al.

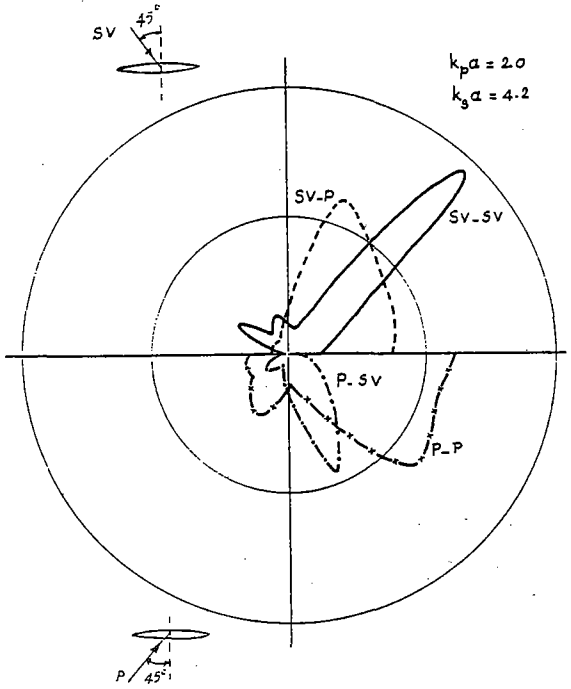

Fig.16 Polar plot of scattered field amplitudes for P -, and SV - waves incident at 45 degrees to an elliptic crack in Al.

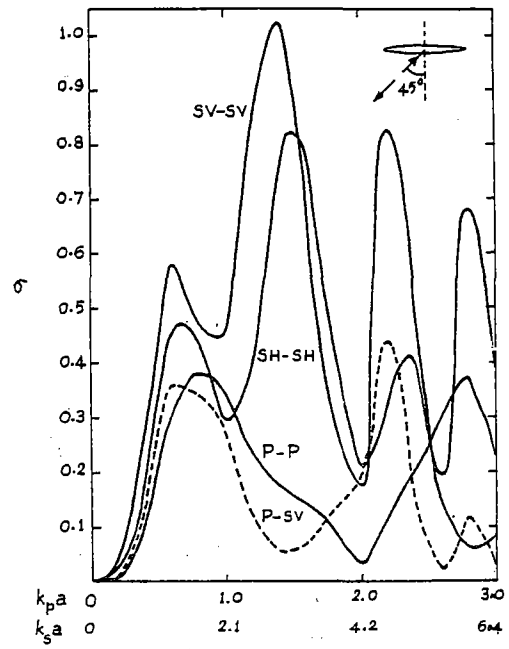

Fig.17 Spectrum of back scattering cross section for P -, SV -, and SH - waves incident at 45 degrees to an elliptic crack in Al.

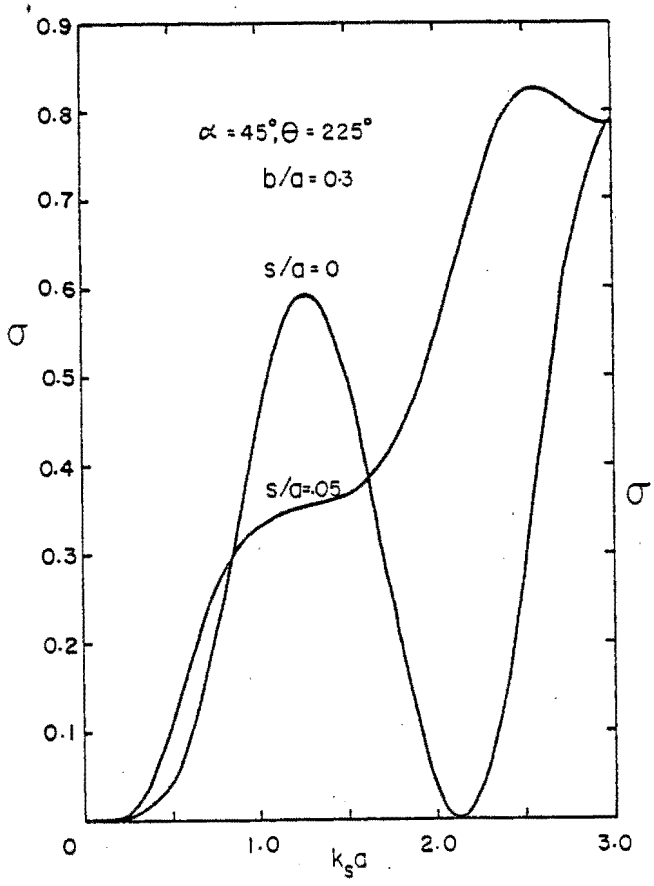

Fig.18 Spectrum of back scattering cross section for SH - waves incident at 45 degrees to the major axis of a rough and smooth ellipse in Al.

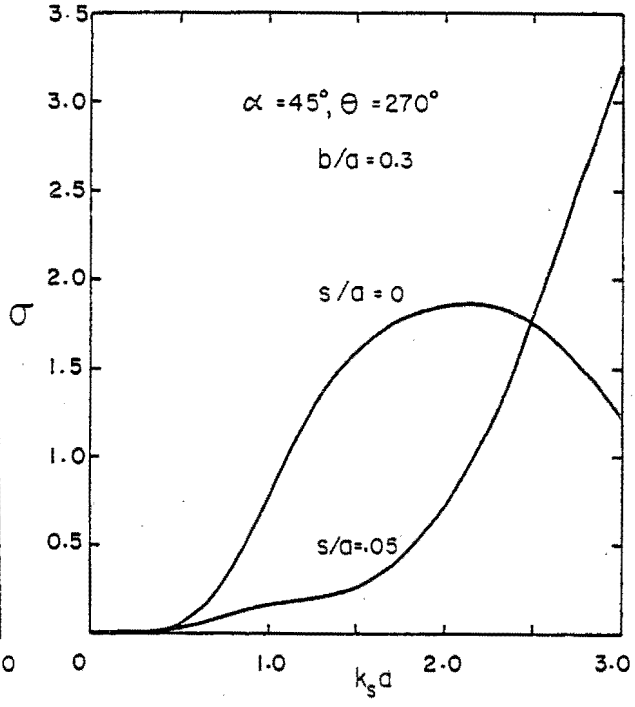

Fig.19 Spectrum of bistatic cross section for SH - waves incident at 45 degrees to the major axis of a rough and smooth ellipse in Al.

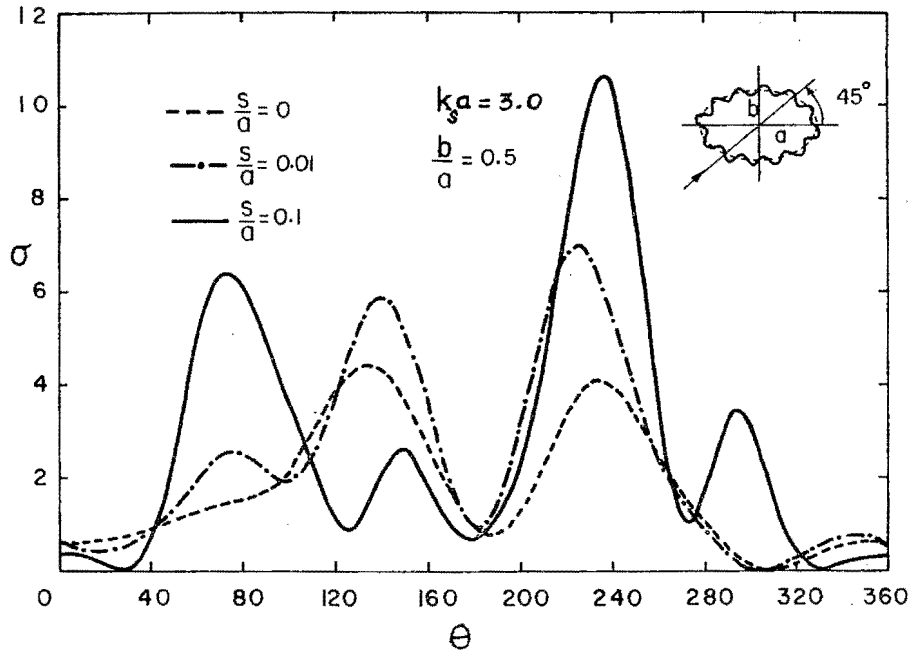

Fig.20 Angular variation of scattered field amplitude for SH - waves incident at 45 degrees to the major axis of a rough ellipse.